Gelsolin Has Three Actin-binding Sites

J. Bryan

Department of Cell Biology, Baylor College of Medicine, Houston, Texas 77030

Abstract. Gelsolin, a Ca^{2+}-modulated actin filament-capping and -severing protein, complexes with two actin monomers. Studies designed to localize binding sites on proteolytic fragments identify three distinct actin-binding peptides. 14NT, a 14-kD fragment that contains the NH_2 terminal, will depolymerize F-actin. This peptide forms a 1:1 complex with G-actin which blocks the exchange of etheno-ATP from bound actin. The estimated association and dissociation rates for this complex are 0.3 μM^{-1} s^{-1} and 1.35×10^{-6} s^{-1} which gives a maximum calculated $K_d = 4.5 \times 10^{-12}$ M. 26NT, the adjacent peptide on the NH_2-terminal half of gelsolin, binds to both G- and F-actin. This fragment has little or no intrinsic severing activity and will bind to F-actin to nearly stoichiometric ratios. The interactions of 14NT and 26NT with actin are largely Ca^{2+} independent and one of these sites, probably 14NT, is the EGTA-stable site identified in the intact protein. 41CT, the COOH-terminal half of gelsolin, forms a rapidly reversible 1:1 complex with actin, $K_d = 25$ nM, that slows but does not block etheno-ATP exchange. This interaction is Ca^{2+} dependent and is the exchangeable site in the intact protein. One of these sites is hidden in the intact protein, but cleavage into half fragments exposes all three and removes the Ca^{2+} dependence of severing.

THE number of actin-binding sites on gelsolin has been generally reported as two (3, 7, 11, 13, 23, 31). We have recently reported that gelsolin can be cleaved into two halves and have shown that the NH_2-terminal half retains a significant fraction of the severing and capping activity of the intact molecule and binds two actin monomers (2). We were unsuccessful in detecting actin binding to the COOH-terminal fragment using HPLC gel filtration methods. Chaponnier et al. (5) have reported a similar cleavage and demonstrated that both the NH_2- and COOH-terminal fragments will bind to G-actin coupled to agarose (5, 16). Binding of the COOH-terminal half was Ca^{2+} dependent and this fragment could be eluted from G-actin-agarose with EGTA. These results led to two quite different proposals for the domain structure of gelsolin and suggested either that the determination of two sites on the NH_2-terminal half of gelsolin was due to actin-actin interactions or that gelsolin had more than two actin-binding sites. We present evidence for the latter case in this report. The NH_2-terminal half of gelsolin can be cleaved into a 14-kD fragment containing the NH_2 terminal and an interior 26-kD fragment. The 14-kD fragment has been reported on previously by Kwiatkowski et al. (16) and demonstrated to retain a small percentage of the severing activity of the whole molecule. We show that this fragment binds tightly to one monomer and will block ATP exchange from this bound actin. The COOH-terminal half also slows ATP exchange from G-actin if Ca^{2+} is present. This confirms the earlier observations of Chaponnier et al. (5). The unexpected observation is that the 26-kD fragment binds to both G- and F-actin in either Ca^{2+} or EGTA. This binding to F-actin is nearly stoichiometric, involves no severing, and clearly is not restricted to filament ends.

Materials and Methods

Large-scale Preparation of Human Plasma Gelsolin

Plasma gelsolin was purified using a modification of a procedure described previously (6). Outdated platelet concentrate was activated by addition of Tris-HCl, pH 7.5, and $CaCl_2$ to 25 mM, followed by warming to 37°C for 45 min. The clotted serum was cooled at room temperature for 1–2 h to allow retraction and then centrifuged at 10,000 *g* for 30 min to remove the clot. The resulting serum was dialyzed against three changes, 4 vol per change, of 25 mM Tris-HCl, 0.5 mM $CaCl_2$, pH 7.5. After dialysis, NaN_3 was added to 1 mM. The dialyzed serum was centrifuged at 25,000 *g* for 30 min to remove aggregated material, adjusted to 35 mM NaCl, and then loaded, at a flow rate of 60 ml/min, onto an 11.5 × 30-cm column of DEAE-Sephacel equilibrated at room temperature with 25 mM Tris-HCl, 50 mM NaCl, 0.5 mM $CaCl_2$, and 1 mM NaN_3, pH 7.5. Usually, the dialyzed serum was frozen and stored at −20°C, then thawed and centrifuged before use. Typically, 1 liter of centrifuged, dialyzed serum was loaded. The first 500–700 ml of eluate was discarded; the next 1,500 ml was collected and cooled to 4°C. EGTA was added to 10 mM and this material was adsorbed to a second DEAE-Sephacel column (11.5 × 8 cm) equilibrated at 4°C with 25 mM Tris-HCl, 50 mM NaCl, 0.1 mM EGTA, and 1 mM NaN_3, pH 7.5. Plasma gelsolin passes through the first column under these conditions, but is adsorbed to the second and can be recovered ~95–98% pure by elution with a 4-liter linear gradient from 0.05 to 0.3 M NaCl. We usually pool the flow through fractions from three runs of the first DEAE column (i.e., 3 liters of serum) and adsorb this to the second DEAE column. The peak material from the gradient is pooled and concentrated by ammonium sulfate precipitation (3.8 g/10 ml of eluate). The essential elements of this purification scheme are the use of sufficient DEAE resin to adsorb the bulk of the serum proteins, particularly albumin, at the first step. We have found 1.5 vol of resin/vol of serum to be adequate, but routinely used ap-

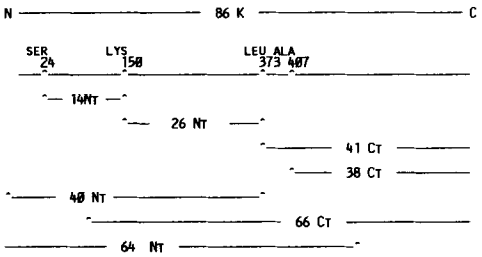

Figure 1. A schematic diagram of a cleavage map of the available human plasma gelsolin fragments. Fragments of gelsolin have been purified from subtilisin, chymotryptic, and tryptic digests and have been designated in various ways (2, 16, 32). The naming convention in the scheme shown above is based on the fragment molecular mass as calculated from protein sequence (17); fragments are further labeled *NT* or *CT* to indicate whether they are derived from the NH_2-terminal or COOH-terminal half of gelsolin, respectively. No designation is made of the proteolytic enzyme used, since most of the fragments can be obtained from different digests or using cloned DNA in bacterial expression vectors. The positions of individual fragments within the gelsolin sequence (17) are based on protein sequence data (2, 5, 16). In general, 14NT, 26NT, 40NT, 41CT, and 38CT can be isolated from limited chymotryptic or subtilisin digests. 14NT and 66CT can be isolated efficiently from limited trypsin digests. 64NT is the product of an unidentified serum protease and accumulates in our antibody-purified gelsolin preparations during storage at 4°C (2). The fragments listed above have previously been designated by SDS gel molecular weights and by an enzyme prefix. The correspondence is as follows: 14NT = CT15, CT17, CT14N; 26NT = CT30, CT31, CT28N; 41CT = CT54, CT47; 38CT = CT45, CT38C; and 64NT = U75.

proximately twice this amount. We have also found that having some salt present, 25–50 mM, improves reproducibility and minimizes gelsolin adsorption to the first DEAE column. The recovery is 80–100 mg of plasma gelsolin after precipitation, dialysis, and centrifugation for 10 min in a microfuge to remove minor amounts of aggregated material. Gelsolin was stored at 4°C in the final dialysis buffer, 10 mM Tris-HCl, 0.1 mM EGTA, pH 7.5, or frozen in liquid nitrogen.

Fragment Purification

We have used several strategies to purify the fragments described here. The conditions for cleavage and isolation of 40NT and 41CT, the NH_2- and COOH-terminal halves, respectively, have been described previously (2). Fig. 1 gives a schematic cleavage map and overview of plasma gelsolin based on available sequencing data and describes the relationships, naming, and origin of the various fragments.

14NT Fragment

The 14-kD fragment, 14NT, containing the NH_2 terminal has been purified from trypsin digests of plasma gelsolin. 25 mg of protein was cleaved with 5 μg of *N*-tosyl-L-phenylalanine chloromethyl ketone (TPCK)-treated trypsin for 3 h at 25°C in 25 mM Tris-HCl, 1 mM NaN_3, and 2.5 mM EGTA at pH 7.5. The trypsin was inactivated by addition of diisopropyl fluorophosphate (DIFP) to a final concentration of 1 mM and the digest was applied to a DEAE-5PW column (Waters Instruments, Inc., Rochester, MN). The 14NT fragment and several other peptides elute in the flow-through fractions when the column is eluted with 25 mM Tris-HCl, 0.2 mM EGTA, pH 7.5. These fractions are collected and concentrated on centricon 10 filters (Amicon Corp., Danvers, MA), then rechromatographed on a Bio-Gel TSK SP-5-PW column (Bio-Rad Laboratories, Richmond, CA). The column was eluted with 25 mM Tris-HCl, 0.2 mM $CaCl_2$, pH 7.5. The 14NT fragment is not adsorbed to the sulfopropyl resin and can be recovered at 95% purity in the flow-through fractions.

26NT Fragment

The 26-kD fragment, 26NT, adjacent to 14NT can be isolated from chymotryptic digests of plasma gelsolin. We routinely digest 50–100 mg of gelsolin with chymotrypsin at a 100:1 wt/wt ratio at 25°C for 90 min in 25 mM Tris-HCl, 0.2 mM $CaCl_2$, pH 8.0. The long cleavage time is used to reduce contamination with the NH_2-terminal half fragment, which has very similar purification properties. Digestion is terminated by addition of DIFP to 1 mM and EGTA to a final concentration of 5 mM. The digest is adsorbed to a Waters DEAE-5PW column equilibrated with 25 mM Tris-HCl, 0.2 mM EGTA at pH 7.5, and eluted with a gradient from 0 to 0.4 M NaCl at a flow rate of 1 ml/min. The 26NT fragment elutes partially in the flow-through and early in the gradient at ~0.025–0.05 M NaCl. Fractions are pooled and concentrated using the centricon 10 filters. After concentration, the sample is diluted with ~10 vol of 25 mM Tris-HCl, 0.2 mM $CaCl_2$; pH 7.5, and rechromatographed on the sulfopropyl resin using a 0–0.4-M NaCl gradient in 25 mM Tris-HCl, 0.2 mM $CaCl_2$, at pH 7.5. The 26NT fragment elutes at ~0.3 M and is again pooled and concentrated using the centricon 10 filters. The major contaminant, <0.1%, at this stage is uncleaved 40NT. This can be reduced if necessary by an additional chymotryptic cleavage and rechromatography cycle using the sulfopropyl resin.

41CT Fragment

The 41-kD fragment, 41CT, can be recovered from the same chymotryptic digests used to isolate 26NT. 41CT is retained more tightly on the DEAE resin and elutes at 0.2–0.25 M NaCl. Fractions are pooled, concentrated, and diluted as described for the 26NT fragment. Chromatography on the sulfopropyl resin can be used as an additional purification step if necessary. 41CT is not retained while 26 and 40NT are tightly bound.

Extinction Coefficients

The concentrations of the fragments were determined using extinction coefficients calculated from sequence data (17) using E^{M}_{280} = 1,340 for tyrosine and E^{M}_{280} = 5,850 for tryptophan (19). The calculated extinction coefficients used were E^{M}_{280} = 21,080 for 14NT; 28,760 for 26NT; 67,390 for 41CT; and 49,840 for 40NT.

Prelabeling of Actin with Etheno-ATP

Etheno-ATP, initially synthesized and characterized by Secrist et al. (24) and demonstrated by Thomas et al. (27) and Miki et al. (20) to show enhanced fluorescence on binding to G-actin, was used to measure nucleotide exchange. Actin was labeled with etheno-ATP (Molecular Probes Inc., Junction City, OR) by gently homogenizing 50–100 mg of F-actin in 0.5 mM etheno-ATP, 2 mM Tris-HCl, 0.2 mM $CaCl_2$, and 1 mM NaN_3 at pH 8. The F-actin was depolymerized overnight at 4°C at a concentration of 5 mg/ml, then centrifuged at 100,000 *g* for 90 min. KCl and $MgCl_2$ were added to final concentrations of 100 and 2 mM, respectively, to initiate polymerization. After 3 h, F-actin was collected by centrifugation at 100,000 *g* for 90 min, then resuspended, depolymerized, and recentrifuged in 2 mM Tris-HCl, 0.2 mM $CaCl_2$, 1 mM NaN_3, pH 8, with 50 μM etheno-ATP. The resulting G-actin was stored at 4°C at a final protein concentration of 50–100 μM. For long-term storage, etheno-ATP-labeled actin was frozen in liquid nitrogen and stored at −80°C. Actin was isolated from rabbit skeletal muscle and gel filtered (18) on Sephadex G-150 as described previously (1).

Fluorescence Measurements

Etheno-ATP fluorescence was measured using an excitation wavelength of 358 nm and an emission wavelength of 407 nm. Kinetic experiments were done using 2.0 ml of 1 μM etheno-ATP G-actin containing 0.5–1 μM free etheno-ATP. The exchange reaction was initiated by addition of 2.5 μl of 0.1 M ATP, a 125–250-fold excess of the unlabeled nucleotide. The sample was continuously illuminated and points were collected automatically. Additional experiments indicated <2% photobleaching took place over a 36-h period with continuous excitation at 358 nm and a 5-nm band width. Excitation and emission spectra were determined for etheno-ATP-labeled actin in the presence and absence of saturating amounts of 14NT and 41CT. No significant differences were found. The concentration of etheno-ATP-labeled actin, εATP actin, present at a given time was calculated from the fluorescence emission data using the following formula:

$$[\varepsilon\text{ATP actin}] = \frac{F(t) - F(\infty)}{F(o) - F(\infty)} \cdot [1\ \mu\text{M}], \qquad (1)$$

where $F(o)$ and $F(\infty)$ are the initial and final fluorescence values of the actin control and $F(t)$ is the fluorescence of the sample at time t. For the con-

trol actin preparations and for those samples that exchange completely (i.e., actin plus 4ICT), the initial and final fluorescence values, $F(o)$ and $F(\infty)$, and the observed rate constant, k_{obs}, were determined by fitting the data to the monoexponential equation:

$$F(t) = F(o)\, e^{-k_{obs}t} + F(\infty). \quad (2)$$

For samples that do not exchange completely (i.e., actin plus 14NT), the kinetic parameters were determined by fitting a variant of this equation:

$$F(t) = F(o)\, e^{-k_{obs}t} + F(f). \quad (3)$$

where $F(f)$ is the final fluorescence value reached by the sample. In either case the fitting was done with 350–500 data points, covering 5–10 half lives of the reaction, using the algorithm described by Jericevic et al. (14).

Kinetic Simulations

Simulation of the various reactions described here, particularly the 14NT–actin interaction and determination of the kinetic constants for this reaction were done using the simulation control programs, SCoP and SCoPfit, developed and distributed by the National Biomedical Simulation Resource, Duke University Medical Center, Durham, NC.

Results

Evidence for Three Actin-binding Sites

We have studied the exchange properties of etheno-ATP from actin after addition of ATP and have used these changes to assess the binding of gelsolin fragments to G-actin. To circumvent the difficulties associated with changes in Ca^{2+} concentration described by Engel and colleagues (22, 29, 30; see also reference 28), the exchange reactions were carried out in a relatively high Ca^{2+} concentration, 800 μM, since preliminary experiments indicated the exchange rate of etheno-ATP from G-actin was insensitive, upon addition of 125 μM ATP, to small Ca^{2+} changes when the Ca^{2+} concentration was between 0.5 and 1 mM.

Interaction of the 14-kD NH_2-terminal Fragment with Actin

Fig. 2 *a* illustrates the block of exchange of etheno-ATP from G-actin by 14NT. Increasing concentrations of the fragment result in higher, stable plateaus indicating unexchanged etheno-ATP. 14NT does not affect the rate of exchange of etheno-ATP from the uncomplexed actin. The calculated k_{obs} for all the measurements was 0.0039 s^{-1} (range = 0.0042–0.0031; n = 12), which was indistinguishable from the observed rate constant for control G-actin solutions under the same conditions. Fig. 2 *b* shows the binding curve derived from a number of titration experiments with actin and 14NT. The concentrations of complex were derived from the final values for etheno-ATP actin obtained 8–10 h after addition of ATP. One series of experiments, illustrated by the open circles, was done by mixing 14NT with actin and incubating at 20°C for 5–7 min. The results are scattered, but can be fit with a binding isotherm with a K_d of ~30 nM. This value is in approximate agreement with that reported by Kwiatkowski et al. (16). In a second series of experiments, illustrated by the solid squares, the samples were mixed and preincubated for a minimum of 4 h (range 4–18 h) to ensure that complex formation was complete before addition of ATP. The results, particularly at the higher 14NT concentrations, suggest that complex formation was not complete in the first series of experiments and that the K_d for 14NT–actin complex formation is considerably <30 nM. We have estimated

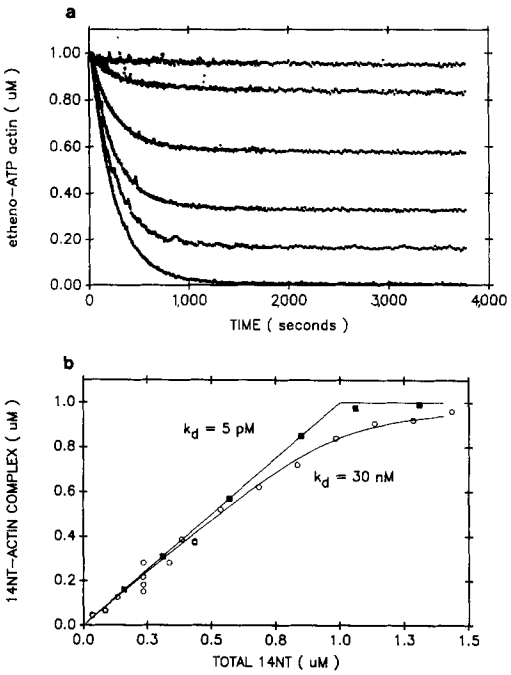

Figure 2. Exchange of etheno-ATP from G-actin in the presence of 14NT. *a* illustrates the exchange of etheno-ATP from 1 μM G-actin after addition of ATP to 125 μM at time = 0. The concentration of etheno-ATP actin was calculated from fluorescence measurements as described in Materials and Methods. The 14NT–actin ratios, beginning with the lowest plateau, are 0, 0.2, 0.4, 0.6, 0.8, and 1.0. the decay constants, k_{obs}, determined using the procedure described in Materials and Methods, were 0.0039 s^{-1} (range = 0.0031–0.0042 s^{-1}) for all of the observed exchanges. The reactions were done in 25 mM Tris-HCl, 800 μM $CaCl_2$, 120 μM $MgCl_2$, and 1 mM NaN_3, pH 8.0 at 20°C. The initial free etheno-ATP concentration was ~1 μM. The dead time for mixing and transfer was ~10–15 s. For this particular experiment the minimum preincubation time was 4 h; for other experiments a minimum time of 5–7 min was used. *b* illustrates a binding curve for the interaction of 14NT with G-actin. The concentration of free 14NT was calculated by subtracting the concentration of complex from total 14NT in the reaction. The solid lines are curves calculated for a 1:1 complex using K_d's of 30 nM and 5 pM, respectively. The open circles are data points obtained with short, somewhat variable preincubations for complex formation of 5–7 min; the solid squares are data points obtained after a minimum of 4 h preincubation.

this equilibrium constant by determining the association and dissociation rate constants for the following scheme:

Scheme I

$$\begin{array}{l} \varepsilon ATP \cdot actin + 14NT + ATP \underset{k_{-2}}{\overset{k_{+2}}{\rightleftharpoons}} 14NT \cdot \varepsilon ATP \cdot actin \\ \qquad\qquad \Big\downarrow \; + ATP,\ k_{-1} \\ ATP \cdot actin + 14NT \underset{k_{-2}}{\overset{k_{+2}}{\rightleftharpoons}} 14NT \cdot ATP \cdot actin, \end{array}$$

where εATP and ATP are the fluorescent and nonfluorescent forms of ATP. We assume that in the presence of excess ATP the rate-limiting step for exchange is the dissociation of etheno-ATP–labeled actin with a rate constant of k_{-1}. Fur-

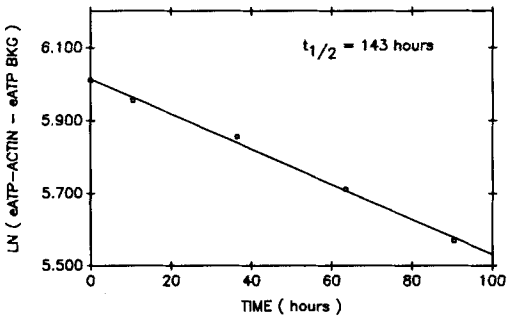

Figure 3. Determination of the dissociation rate constant, k_{-2}, of the 14NT-actin complex. The dissociation of the 14NT-actin complex was determined by monitoring the fluorescence decrease as a function of time assuming no exchange from the complex. Complexes were formed as described in Fig. 2. The mixtures had 14NT/actin ratios of 0.2, 0.4, 0.6, 0.8, and 1.0; the fluorescence values were followed for ~4 d at 20°C. Semilog plots of the fluorescence values vs. time gave straight lines with nearly equal slopes. The data shown are the averages of values at each time point. The average $t_{½}$ is 143 h or $k_{-2} = 1.35 \times 10^{-6}$ s^{-1}. The individual values of k^{-2}, at the different 14NT/actin ratios, range from 1.30 to 1.41 $\times$ 10^{-6} s^{-1}. These calculations assume that nucleotide exchange only occurs from free G-actin, not from the 14NT-actin complex.

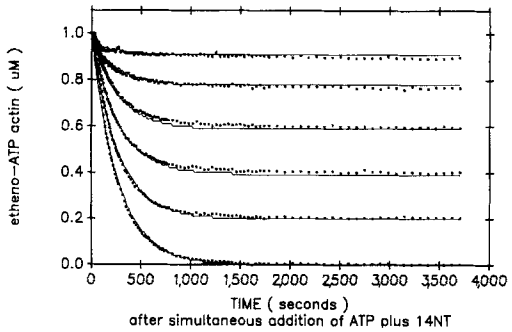

Figure 4. Determination of the association rate, k_{+2}, of the 14NT-actin complex. The association rate constant for 14NT-actin complex formation was determined by measuring the rate of inactivation of nucleotide exchange after simultaneous addition of ATP and 14NT to etheno-ATP actin. The data shown are for reactions with 14NT/actin ratios of 0, 0.2, 0.4, 0.6, 0.8, and 1.0. The data were interpreted using Scheme I and assuming that the dissociation of the complex was negligible over the time of the analysis; i.e., $k_{-2} = 0$. The actual analysis was done using the computer program described in Materials and Methods. This entails defining a model. In this case the definition consists of writing down the five differential equations that specify the changes in the protein species in Scheme I. The SCoPfit program does a global least squares fit of k_{+2} and k_{-1} to all of the data from experiments at the various 14NT/actin ratios. The values obtained, $k_{+2} = 0.299$ μM^{-1} s^{-1} and $k_{-1} = 0.00374$ s^{-1}, were independent of the initial estimates, step sizes, and error function used by the SCoPfit program. In addition, the value of k_{-1} is in agreement with the values determined in Fig. 2 using a nonlinear least squares procedure (14). The open symbols are the data points; the solid lines were calculated using the best fit values. The solution conditions are the same as those given in Fig. 2.

thermore, we assume that 14NT binds equally to etheno-ATP and ATP actin. We have estimated the three kinetic constants, k_{-1}, k_{+2}, and k_{-2} as described below.

The dissociation rate of 14NT etheno-ATP-labeled actin, k_{-2}, was estimated by monitoring the long-term fluorescence change of complexes after ATP addition. The result of one series of experiments is shown in Fig. 3. In this experiment, five reaction mixtures, similar to those shown in Fig. 2, were followed for 4 d. The mixtures had 14NT/actin ratios of 0.2, 0.4, 0.6, 0.8, and 1.0. Semilog plots of fluorescence vs. time gave straight lines with approximately equal slopes; therefore, the data were averaged at each time point. These data give a $t_{½}$ of 143 h or $k_{-2} = 1.35 \times 10^{-6}$ s^{-1}. The individual values range from 1.30 to 1.41 $\times$ 10^{-6} s^{-1}. The implicit assumption in this experiment is that nucleotide exchange can only occur from free actin.

The association constant, k_{+2}, and the dissociation rate of etheno-ATP from G-actin, k_{-1}, were estimated at the same time using the numerical simulation program, SCoPfit, described in Materials and Methods. Experimentally, the approach was to mix etheno-ATP-labeled actin simultaneously with 14NT and ATP and monitor the fluorescence change. The fluorescence data were converted to etheno-ATP-labeled actin concentrations as described in Materials and Methods. The data were analyzed by defining a model based on Scheme I with the additional assumption that the dissociation of the 14NT-actin complex was negligible over the course of the experiment; i.e., $k_{-2} = 0$. This assumption is not restrictive; including the value of k_{-2} determined above does not alter the results. Defining the model consists of writing the five differential equations that specify changes in each of the five protein species; changes in ATP do not enter into the model. The SCoPfit program was used to minimize a least squares function by adjusting the values of k_{+2} and k_{-1}. One data set is shown in Fig. 4. The open squares are data points; the solid lines are the least squares fit derived from the entire data set. The 14NT/actin ratios used were 0, 0.2, 0.4, 0.6, 0.8, and 1.0. The least squares values for the data set were $k_{+2} = 0.299$ μM^{-1} s^{-1} and $k_{-1} = 0.00374$ s^{-1}. The k_{-1} value is in agreement with the data from Fig. 2 *a* determined using a nonlinear least squares procedure. The calculated equilibrium constant for 14NT-actin complex formation is given by $K = k_{+2}/k_{-2} = 2.2 \times 10^{11}$ M^{-1} or a K_d of ~4–5 pM. As outlined in the Discussion, this is a maximum estimate of the K_d. The simulation procedures were run using a variety of initial conditions, step sizes, and error functions, all of which gave convergence to a similar set of rate constants.

We have investigated the effects of EGTA on the reaction. At low Ca^{2+} concentrations (i.e., in 1–5 mM EGTA), the displacement of nucleotide is biphasic; the fast phase has the same rate constant as the G-actin controls, while the slow phase decays at ~1–2% of this rate, $k_{obs} = 0.0003$ s^{-1} vs. 0.02 s^{-1}. This slow phase is ~225-fold faster than the value of k_{-2} in Ca^{+2}. We have estimated the fast component in the presence of EGTA and used this to derive a binding plot. Half-maximal saturation is at 1–2 nM 14NT. This suggests the formation of the 14NT-actin complex is not strongly Ca^{2+} dependent. We have interpreted this to mean that the rate of nucleotide exchange from the complex is mediated by Ca^{2+}. Complex formation also can be demonstrated in EGTA using gel filtration (data not shown). The reasons for the increased rate of exchange for etheno-ATP from the 14NT-actin complex in EGTA are not clear, but could involve the replacement of Ca^{2+} on the actin by Mg^{2+} at either

the moderate-affinity sites (33) or the high-affinity site (4, 9, 33), hydrolysis of ATP (26), or direct Ca^{2+} binding to 14NT.

Interaction of the 41-kD COOH-terminal Fragment with Actin

Fig. 5 *a* illustrates the effects of the 41-kD COOH-terminal fragment, 41CT, on the exchange of etheno-ATP from actin. Increasing the concentration of 41CT does not alter the final fluorescence values but does slow the rate of exchange in a concentration-dependent fashion. The data points are fit reasonably by a monoexponential function; the semilogarithmic plots of $F(t) - F(\infty)$ vs. time are all linear. This type of behavior suggests that 41CT reacts rapidly and reversibly with G-actin. We have interpreted these results in terms of a scheme similar to that used by Mockrin and Korn (21) to describe the effects of profilin on ATP exchange from G-actin. This is shown below:

Scheme II

$$\varepsilon\text{ATP} \cdot \text{actin} + 41\text{CT} \underset{K_1}{\rightleftharpoons} 41\text{CT} \cdot \varepsilon\text{ATP} \cdot \text{actin}$$

$$k_{+1} \quad k_{-1} \quad +\text{ATP} \qquad k_{-2} \quad +\text{ATP} \quad k_{+2}$$

$$\text{ATP} \cdot \text{actin} \underset{K_1}{\rightleftharpoons} 41\text{CT} \cdot \text{ATP} \cdot \text{actin}.$$

ATP and εATP are the nonfluorescent and fluorescent forms of ATP, respectively. The Mockrin–Korn model assumes a rapid, reversible 1:1 interaction between G-actin and the binding protein. The model also assumes that the k_{+1} and k_{+2} pathways can be ignored because the concentration of etheno-ATP is low relative to the total. Therefore, once dissociation of a fluorescent molecule has occurred there is little opportunity for its reassociation. As indicated by Mockrin and Korn (21), within these constraints the dissociation of ATP can be described by the first-order equation:

$$-\frac{d\,(\varepsilon\text{ATP} \cdot \text{actin})}{dt} \tag{4}$$

$$= \frac{k_{-1} + k_{-2}\,[41\text{CT}] / K_1}{1 + [41\text{CT}] / K_1} \cdot (\varepsilon\text{ATP} \cdot \text{actin})$$

$$= k_{obs}\,(\varepsilon\text{ATP} \cdot \text{actin}).$$

These authors derive a second equation, not shown, which allows a plot of $1/(k_{-1} - k_{obs})$ vs. 1/[profilin] to be used to determine k_{-2} and K_1 from the intercept and slope. The profilin–actin interaction is sufficiently weak that all of the added profilin can be considered unbound. Similar double reciprocal plots using the total 41CT concentration show a marked nonlinearity because the association constant is higher. We have, therefore, reformulated equation 4 in terms of the total concentrations of G-actin and 41CT and used this to estimate the parameters in Scheme II. This was done using the conservation relations

$$[41\text{CT}]_T = [41\text{CT}]_F + [\text{COMPLEX}] \tag{5}$$

and

$$[\varepsilon\text{ATP} \cdot \text{actin}]_T = [\varepsilon\text{ATP} \cdot \text{actin}]_F + [\text{COMPLEX}] \tag{6}$$

and the dissociation constant

$$K_1 = \frac{[41\text{CT}]_F\,[\varepsilon\text{ATP} \cdot \text{actin}]_F}{[\text{COMPLEX}]}, \tag{7}$$

where the T and F subscripts indicate total and free concentrations and [COMPLEX] = [41CT–etheno-ATP-labeled actin]. The final equation used to fit the data by minimizing a least squares function is

$$K_{obs} = \frac{k_{-1} + \frac{k_{-2}}{K_1}\,([41\text{CT}]_F - [\text{COMPLEX}])}{1 + \frac{1}{K_1}\,([41\text{CT}]_T - [\text{COMPLEX}])}, \tag{8}$$

where

$$[\text{COMPLEX}] = \frac{\alpha \pm \sqrt{\alpha^2 - 4[\varepsilon\text{ATP} \cdot \text{actin}]_T[41\text{CT}]_T}}{2} \tag{9}$$

and

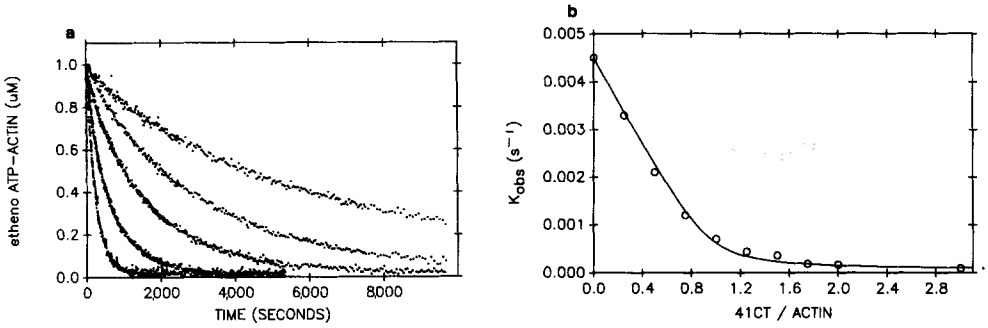

Figure 5. Exchange of etheno-ATP from G-actin in the presence of 41CT. *a* illustrates the exchange of etheno-ATP from 1 μM G-actin after addition of ATP to 125 μM at time = 0. The concentration of etheno-ATP actin was calculated from the fluorescence measurements as described in Materials and Methods. The 41CT–actin ratios, beginning with the fastest reaction, were 0, 0.5, 1.0, 1.5, and 2.0. The reactions were done in 25 mM Tris-HCl, 800 μM $CaCl_2$, 120 μM $MgCl_2$, and 1 mM NaN_3, pH 8.0 at 20°C. *b* illustrates the effect of 41CT on the rate constants, k_{obs}, obtained by fitting the data in *a* to the monoexponential equation given in Materials and Methods. The initial slope extrapolates to a value of one 41CT interacting with one actin monomer. The solid line was calculated for k_{obs} values defined by equations 8, 9, and 10 in the text, based on Scheme I. The best fit values used for the solid line were K_1, the equilibrium dissociation constant for the complex (25 nM); k_{-1}, the dissociation rate constant for etheno-ATP from G-actin (0.0045 s^{-1}); and k_{-2}, the dissociation rate constant for etheno-ATP from the 41CT–actin complex (0.00005 s^{-1}).

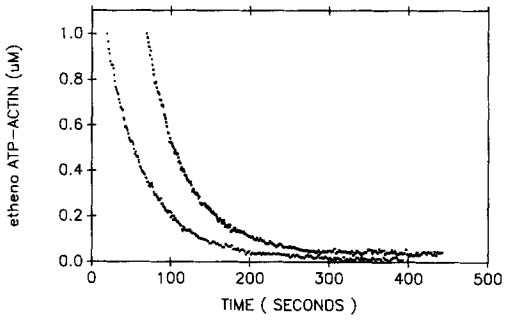

Figure 6. The 41CT effect on etheno-ATP exchange from G-actin is Ca^{2+} dependent. Exchange experiments were done as described in Fig. 5 with no added $CaCl_2$ in 25 mM Tris-HCl, 120 μM $MgCl_2$, 2.5 mM EGTA, and 1 mM NaN_3 at pH 8.0. The 41CT sample contained 5 μM 41CT, a 5:1 ratio with actin. The control actin values are represented by the left curve; the 41CT + actin values by the right curve. The mixture data are offset 50 s from the control for purposes of illustration.

$$\alpha = [\varepsilon ATP \cdot actin]_T + [41CT]_T + K_1. \qquad (10)$$

The results are shown as a binding curve in Fig. 5 *b* for one data set. The calculated best fit values for k_{obs} as a function of the total 41CT per actin ratio are given by the solid line for $K_1 = 25$ nM, $k_{-1} = 0.0045\ s^{-1}$ and $k_{-2} = 0.00005\ s^{-1}$. Note also that the initial binding curve extrapolates to a value of one 41CT per actin. The estimated dissociation constant agrees reasonably well with the determination (Weber, A., J. Bryan, M. Mooseker, and H. Rosenbaum, unpublished observations) using a completely independent method.

Dependence of the 41CT-Actin Interaction on Ca^{2+} Concentration

Fig. 6 demonstrates that 41CT does not affect the exchange of etheno-ATP from actin in the presence of EGTA. The k_{obs} values for exchange are equal to the control values in the presence of a fivefold molar excess of 41CT. It is possible to demonstrate formation of a 41CT-actin complex using gel filtration. There is a shift in the elution position of G-actin + 41CT, mixed in a 1:1 ratio at an initial concentration of 30 μM, when chromatographed on a G-75 column equilibrated with 2 mM Tris-HCl, 1 mM $MgCl_2$, and 800 μM $CaCl_2$, pH 8.0. We observe no shift with 5 mM EGTA present.

Interaction of the 26-kD NH_2-terminal Fragment with F-Actin

The 26-kD fragment, 26NT, adjacent to 14NT on the NH_2-terminal half of gelsolin was shown to bind to F-actin using a sedimentation assay. The results of one set of experiments where 5 μM actin was mixed with varying concentrations of 26NT is shown in Fig. 7. We observe binding in either Ca^{2+} (0.2 mM) or EGTA (2.5 mM) in 0.1 M KCl, 2 mM $MgCl_2$, 0.5 mM ATP, 1 mM NaN_3, 2 mM Tris-HCl at pH 7.5. Densitometry of the gels and of known amounts of actin and 26NT was done to quantitate this binding. The results, as a simple binding curve, are shown in Fig. 8. We have not obtained 1:1 saturation of the actin monomers in the filaments,

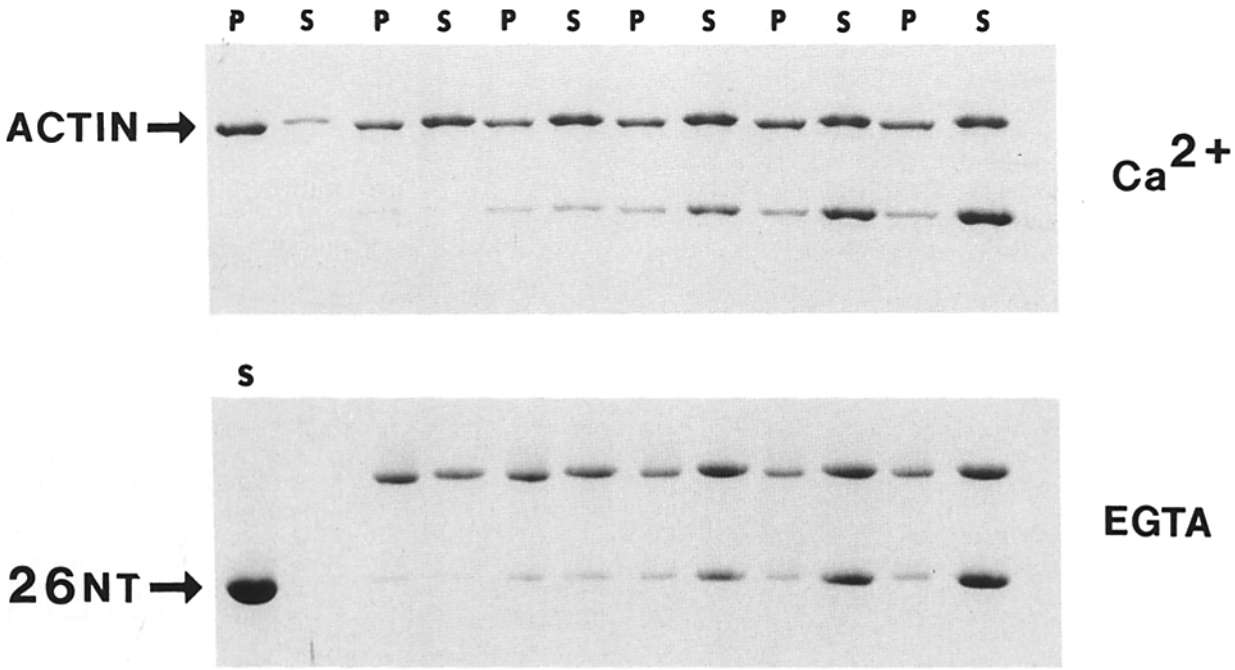

Figure 7. Interaction of 26NT with F-actin. A solution of F-actin at a final concentration of 5 μM was mixed with increasing concentrations of 26NT. After 60 min at 25°C, the samples were centrifuged in an airfuge (Beckman Instruments, Inc., Palo Alto, CA) at 30 psi for 30 min. Supernatants and pellets were separated and analyzed by SDS-PAGE. The results for binding in 100 mM KCl, 2 mM $MgCl_2$, 0.5 mM ATP, 0.2 mM $CaCl_2$, and 2 mM Tris-HCl at pH 7.5 are shown in the upper panel. The lower panel shows the results for a similar experiment without $CaCl_2$ with 2.5 mM EGTA added. *P*, pellet fraction; *S*, supernatant fraction. The left two lanes in the upper panel are the actin control in the absence of 26NT. The final concentrations of 26NT, from left to right, are 0.5, 1.5, 3.0, 4.5, and 6.0 μM. The left two lanes in the lower panel are the 26NT control; the lanes are reversed, and the prominent 26NT band is in the supernatant. Under these conditions essentially no 26NT is observed in the pellet.

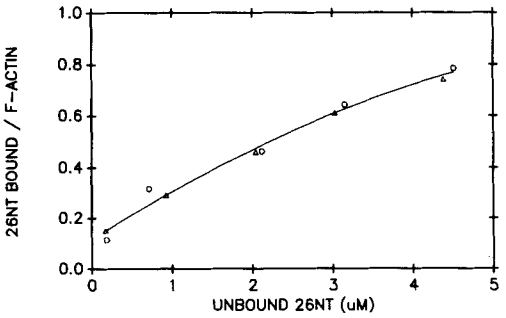

Figure 8. Quantitation of 26NT binding to F-Actin. The Coomassie Blue-stained gels shown in Fig. 5 were analyzed by densitometry and compared with known amounts of 26NT and skeletal muscle actin stained at the same time. The concentration of free 26NT was calculated by subtracting the amount bound from the total 26NT in the reaction mixture. The data are plotted as a simple binding curve for the 26NT-actin interaction. (○) With calcium; (△) without calcium.

suggesting there is some hindrance with increasing occupancy. This is reflected in nonlinear Scatchard plots (data not shown). Electron microscopy of filaments made at a 1:1 ratio of 26NT to actin show linear structures, somewhat thicker than typical F-actin, missing the distinctive helical crossover pattern. There is no difference in the extent of binding of 26NT to F-actin in the presence of either Ca^{2+} or EGTA.

We have been unable to determine whether 26NT has intrinsic capping activity since it has been very difficult to remove uncleaved 40NT, the NH_2-terminal half fragment of gelsolin that efficiently severs and caps filaments (2). The problem is that we are using micromolar concentrations of 26NT to assay binding, while subnanomolar concentrations of the 40NT fragment sever and cap effectively. The preparations used here raise the critical concentration somewhat more than is expected for a simple capping activity, but consistent with some severing activity. 26NT does not have an intrinsic severing activity since there are sedimentable filaments even at ratios of 26NT/actin monomer >1. Preliminary depolymerization experiments with pyrene-labeled F-actin suggest that the 26NT fragment may protect against the severing activity of residual 40NT. We are trying to study these effects more thoroughly using highly purified 26NT.

Interaction of 26NT with G-Actin

We have looked for interactions between 26NT and G-actin using gel filtration. Fig. 9 demonstrates the chromatographic behavior of 26NT, G-actin, and a 1.3:1 mixture of 26NT and G-actin on G-75 Sephadex in G-buffer (2 mM Tris-HCl, 0.2 mM $CaCl_2$, 0.5 mM ATP, 1 mM NaN_3 at pH 8.0). The G-actin concentration was 28 μM. In the mixture experiment, the actin elutes quantitatively in the void volume of the column. The results demonstrate an interaction between 26NT and G-actin in the presence of Ca^{2+}. Similar experiments (data not shown) using G-actin preequilibrated with 2 mM Tris-HCl, 2.5 mM EGTA, 50 μM $MgCl_2$, 0.5 mM ATP, pH 8, and 26NT dialyzed against 2 mM Tris-HCl, 0.2 mM EGTA, pH 8 gave essentially the same results except ~20–25% of the actin control eluted in the column void volume. In the mixture, the actin elutes quantitatively with 26NT. The results demonstrate an interaction in both Ca^{2+}- and EGTA-containing buffers. In these experiments, the complexes are in the void volume of G75. Other preliminary experiments suggest that these complexes are large and elute in the void volume from agarose gel filtration columns with

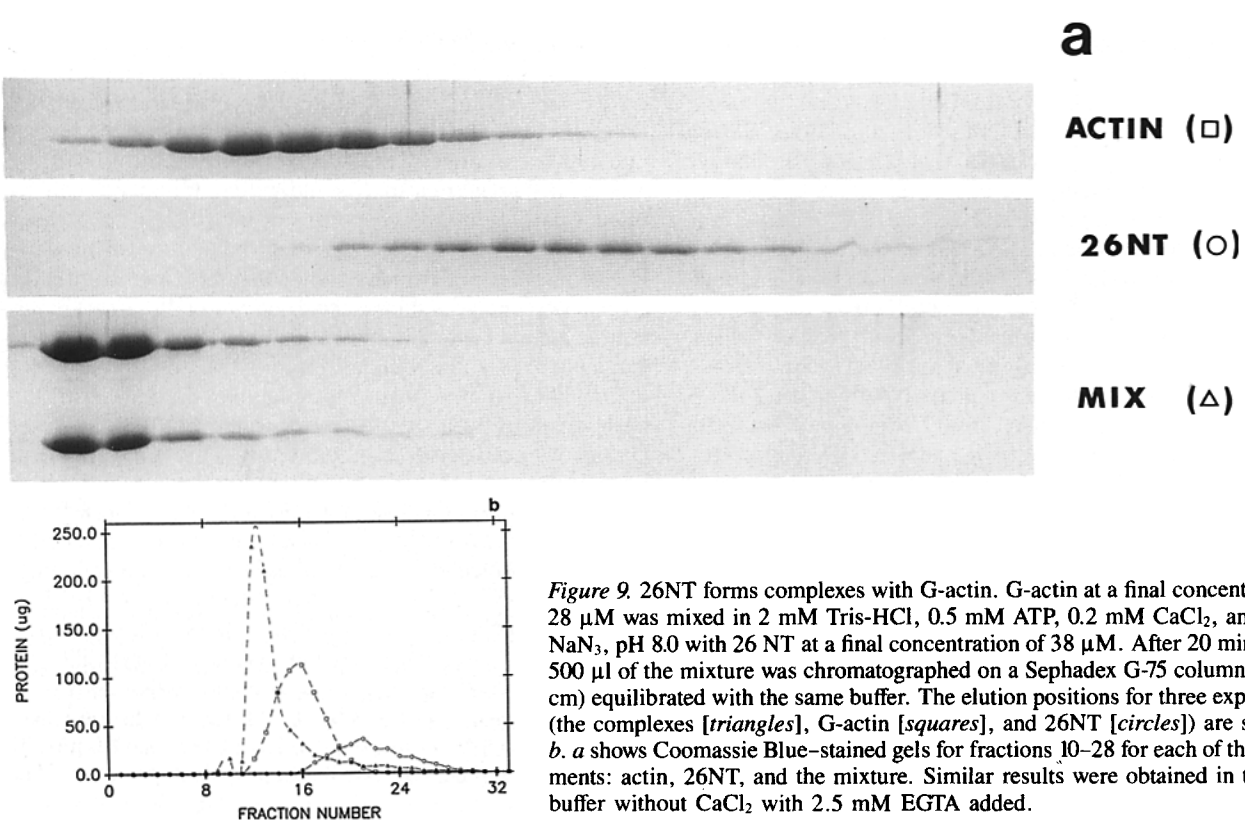

Figure 9. 26NT forms complexes with G-actin. G-actin at a final concentration of 28 μM was mixed in 2 mM Tris-HCl, 0.5 mM ATP, 0.2 mM $CaCl_2$, and 1 mM NaN_3, pH 8.0 with 26 NT at a final concentration of 38 μM. After 20 min at 4°C, 500 μl of the mixture was chromatographed on a Sephadex G-75 column (1 × 50 cm) equilibrated with the same buffer. The elution positions for three experiments (the complexes [*triangles*], G-actin [*squares*], and 26NT [*circles*]) are shown in *b*. *a* shows Coomassie Blue-stained gels for fractions 10–28 for each of the experiments: actin, 26NT, and the mixture. Similar results were obtained in the same buffer without $CaCl_2$ with 2.5 mM EGTA added.

an exclusion limit for globular proteins >2 million. Our preliminary electron microscope observations indicate the formation or stabilization of short actin filaments in these mixtures.

Discussion

The present results indicate that gelsolin has three different domains that bind to and interact with actin in distinct ways. These findings reconcile the reports of Bryan and Hwo (2) and Kwiatkowski et al. (16) and place two of these binding sites on the NH_2-terminal half of the molecule and one on the COOH-terminal half. The NH_2-terminal sites appear to be largely Ca^{2+} insensitive while the COOH-terminal site requires Ca^{2+} for binding. These three actin-binding domains can be purified from partial proteolytic digests and studied in isolation (2, 16, 32).

We have made extensive use of the fact that 14NT and 41CT affect the exchange of etheno-ATP from actin and have used these effects to study the binding parameters of these fragments with actin. This ATP derivative was synthesized initially by Secrist et al. (24), who described its spectroscopic and fluorescence properties. Thames et al. (27) and Miki et al. (20) first used this compound with actin. Engel and colleagues (22, 29, 30; see also reference 28) have used etheno-ATP to show that the exchange of ATP from G-actin is a first-order reaction (29), while ADP exchange is biphasic (22). Nucleotide exchange is slowed by increased Ca^{2+} and increased at higher ATP concentrations (22, 29). Mg^{2+} has been reported to increase the rate of exchange (10). Frieden and Patane (10) have reinvestigated the exchange reactions and proposed a mechanism to account for the biphasic release of ADP and the effects of Mg^{2+} and Ca^{2+} on the reactions.

I have studied the effects of gelsolin peptides on etheno-ATP exchange at high Ca^{2+} concentrations. Under these conditions 14NT binding to actin drastically slows or stops nucleotide exchange. I have interpreted the results in terms of Scheme I. The rate constant for the formation of the slowly exchanging species, k_{+2}, is estimated at 0.3 μM^{-1} s^{-1} and its dissociation rate constant, k_{-2}, at 1.35×10^{-6} s^{-1}. The calculated association constant is 2.2×10^{11} M^{-1}. This is a minimum value since the model assumes there is no nucleotide exchange from the 14NT-actin complex itself and that exchange will only occur when the complex dissociates. This consideration presents a major unresolved problem when trying to determine the sensitivity of the 14NT-actin interaction to Ca^{2+} using nucleotide exchange. We think the 14NT-actin interaction is Ca^{2+} insensitive because we can form the complex in the presence of 1–5 mM EGTA and isolate the complex by gel filtration in EGTA-containing buffers, and because preliminary estimates of k_{+2} in the presence of EGTA are the same as in Ca^{2+}. However, in EGTA we estimate k_{-2} at $\sim$0.0003 s^{-1} for a maximum K_d of $\sim$1 nM vs. 4–5 pM in Ca^{2+}. We cannot, however, rule out more rapid exchange from the complex under these conditions. Therefore, in EGTA, the exchange data are consistent either with a weaker 14NT-actin interaction or an increased rate of nucleotide exchange from the 14NT-actin complex. The calculated K_d for complex formation in Ca^{2+} is considerably lower than that reported by Kwiatkowski et al. (16), but is in the same order as that estimated for the capping constant by Selve and Wegner (25) and for formation of the EGTA-stable complex by Bryan and Kurth (3).

The COOH-terminal half of gelsolin, 41CT, has a distinctly different effect on nucleotide exchange. The results can be interpreted in terms of the rapid equilibrium model shown in Scheme II, with an equilibrium dissociation constant, K_1, of 25 nM and an $\sim$100-fold slower rate of exchange from the 41CT-actin complex than from G-actin. This reaction is markedly Ca^{2+} sensitive; I am unable to detect any effect of 41CT on nucleotide exchange from actin in EGTA. The value of K_1 is in agreement with the 30 nM value determined previously for the binding of a second actin to the EGTA-stable actin–gelsolin complex (3).

The binding properties of the 26NT fragment are the most poorly defined. Binding was observed to both F- and G-actin. In 100 mM KCl, 2 mM $MgCl_2$, pH 7.5, I observed near stoichiometric binding to F-actin which is independent of the Ca^{2+} concentration. The binding curves are not simple and the Scatchard plots are not linear. By contrast, Yin et al. (32) report simple binding with a linear Scatchard plot giving a K_d of $\sim 2 \times 10^{-7}$ after iodination of 26NT. These authors also show that binding of 26NT is sensitive to phosphatidylinositol 4-phosphate and phosphatidylinositol 4,5-bisphosphate. Our preliminary experiments with iodinated 26NT confirm the complex-binding behavior shown in Figs. 7 and 8. The differences are important since the 26NT fragments have been prepared quite differently. Yin et al. (32) purify 26NT by adsorption to G-actin agarose at low salt and elution with 100 mM NaCl, while I used ion exchange chromatography. The actin chromatography step may either select for a particular form of 26NT or displace bound lipid(s) from the actin-binding site.

I found that 26NT promotes the aggregation of G-actin in low ionic strength buffers into large complexes. Preliminary electron microscopic data indicate filament formation suggesting that the 26NT fragment will stabilize F-actin at low ionic strength. These observations make a determination of the 26NT binding parameters by nucleotide exchange difficult since F-actin is known to have a markedly slower nucleotide exchange than G-actin.

The characteristics of the individual fragments can be related partially to the properties of intact gelsolin. Several pieces of evidence suggest that 14NT has the "severing" site. Kwiatkowski et al. (16) have shown that this fragment retains a small percentage of the severing activity of the parent molecule as judged by depolymerization assays. In addition, a 3/4 fragment of gelsolin, which is missing the 14NT-binding domain will cap filaments and block depolymerization from the barbed end in a Ca^{2+}-dependent manner, but will not sever (Bryan, J., manuscript in preparation). This is the fragment labeled 66CT in Fig. 1. I also argue that the 14NT actin-binding domain is the EGTA-stable site defined previously in the parent molecule (3, 15), because the 14NT-actin complex can be formed and isolated in EGTA. The actin-binding domain on 26NT is also a potential candidate for the EGTA-stable site since it is not Ca^{2+} sensitive. However, its affinity for actin is considerably lower than 14NT and, in addition, Kwiatkowski et al. (16) have demonstrated that 26NT is eluted from G-actin agarose by 0.1 M NaCl, while the actin–gelsolin binary complex is stable in EGTA in 0.5–1.0 M NaCl (15). The Ca^{2+}-sensitive, actin-binding domain on 41CT has the characteristics of the Ca^{2+}-sensitive, ex-

changeable site on intact gelsolin. The estimated K_d for the isolated domain, 25 nM, is in excellent agreement with the value, 30 nM, determined for the reaction $GA_1 + A \rightleftharpoons GA_2$ (3).

There have been three reports that intact gelsolin alters the exchange of ATP from G-actin. Harris (12) and Tellam (26) have reported that one of the ATP molecules in the gelsolin–$(actin)_2$ ternary complex is nonexchangeable. Coue and Korn (8), on the other hand, have reported that neither ATP exchanges from the ternary complex. Tellam (26) used etheno-ATP loading experiments to study the effect of gelsolin on nucleotide exchange from actin. We have confirmed his results using washout experiments to show that the ternary complex has two bound ATP molecules, only one of which is exchangeable. The exchange rate is dependent on the gelsolin concentration suggesting that actin-binding at one site is rapidly reversible. The results are qualitatively similar to what I report here for 41CT. The EGTA-stable binary complex contains only a single nonexchangeable ATP, indicating that binding at the exchangeable site is Ca^{2+} dependent (26). Taken together, the results strongly suggest that the COOH-terminal actin-binding domain, localized on 41CT, is occupied in the ternary complex and is the "exchangeable" site, and that the 14NT actin-binding domain is occupied and is the "nonexchangeable" site. The evidence that intact gelsolin has two actin-binding sites and forms a ternary complex is strong (3, 7, 8, 11, 13, 23, 31), ranging from fluorescence measurements (3) through sedimentation equilibrium determinations (8). Therefore, we would conclude that the actin-binding domain on 26NT is not normally occupied in the ternary complexes formed with intact gelsolin under the experimental conditions used. One alternative possibility is that the three domains are distributed spatially to form two compound binding sites in the intact molecule. What we know at this stage is that cleavage to produce the half fragments exposes all three sites. In addition, the 26NT site appears to be required for high-affinity binding to F-actin (i.e., $K_{cap} > 10^{10}\ M^{-1}$) and efficient severing since 40NT and 66CT show high-affinity capping while 14NT and 41CT both have K_{cap} values near 10^7–$10^8\ M^{-1}$ (Weber, A., J. Bryan, M. Mooseker, and H. Rosenbaum, unpublished observations).

How these three sites function sequentially during filament severing is not clear. Intact gelsolin is relatively unreactive toward actin in the absence of Ca^{2+}, even though both NH_2-terminal binding sites are Ca^{2+} independent. This argues that Ca^{2+} binding must cause a molecular change that exposes one or both of the NH_2-terminal sites. Uncovering the 26NT site would promote lateral binding to F-actin and position the 14NT severing site. Phosphatidylinositol 4,5-bisphosphate binding at or near the actin-binding site on 26NT has been proposed to block this lateral binding (32). What actually causes filament breakage is uncertain. I propose that after gelsolin binds laterally to a filament via the 26NT domain, the binding of the 14NT domain induces or stabilizes an actin conformation with markedly weaker actin–actin bonds leading to filament breakage. The blocked ATP exchange of actin bound at the 14NT domain is a reflection of this conformational change. This predicts that a stoichiometric amount of 14NT will bind to and depolymerize F-actin, which it does (16). Similarly, high-affinity capping requires that the 14NT–actin complex remain bound at the filament end. This could occur normally through the 26NT–F-actin binding domain. The need for the 41CT binding site is not clear, but it appears to be necessary to stabilize high-affinity capping in the 3/4 COOH-terminal fragment, 66CT, missing the severing site. x-ray crystallography will be necessary to resolve completely the relationship of the three individual sites to the two actin molecules bound to intact gelsolin in solution and to define the structure of a gelsolin cap at the barbed end of an actin filament.

The author wishes to thank Dr. Carl Frieden for preprints of his papers on etheno-ATP exchange; Brenda Cipriano for manuscript preparation; and Robyn Lee, Wen-Chen Lin, and Shuying Hwo for excellent technical assistance.

This work was funded by National Institutes of Health grants GM26091 and HL26973.

Received for publication 7 August 1987, and in revised form 19 January 1988.

References

1. Bryan, J., and L. M. Coluccio. 1985. Kinetic analysis of F-actin depolymerization in the presence of platelet gelsolin and gelsolin-actin complexes. *J. Cell Biol.* 101:1236–1244.
2. Bryan, J., and S. Hwo. 1986. Definition of an NH_2-terminal actin-binding domain and a COOH-terminal Ca^{2+} regulatory domain in human brevin. *J. Cell Biol.* 102:1439–1446.
3. Bryan J., and M. C. Kurth. 1984. Actin-gelsolin interactions: evidence for two actin-binding sites. *J. Biol. Chem.* 259:7480–7487.
4. Carlier, M., D. Pantaloni, and E. Korn. 1986. Fluorescence measurements of the binding of cations to high-affinity and low-affinity sites on ATP-G actin. *J. Biol. Chem.* 261:10778–10792.
5. Chaponnier, C., P. A. Janmey, and H. L. Yin, 1986. The actin filament-severing domain of plasma gelsolin. *J. Cell Biol.* 103:1473–1481.
6. Cooper, J. A., J. Bryan, B. Schwab III, C. Frieden, and D. J. Loftus. 1987. Microinjection of gelsolin into living cells. *J. Cell Biol.* 104:491–501.
7. Coue, M., and E. D. Korn. 1985. Interaction of plasma gelsolin with G-actin and F-actin in the presence and absence of calcium ions. *J. Biol. Chem.* 260:15033–15041.
8. Coue, M., and E. D. Korn. 1986. ATP-hydrolysis by the gelsolin-actin complex and at the pointed ends of gelsolin-capped filaments. *J. Biol. Chem.* 261:1588–1593.
9. Estes, J. E., L. A. Selden, and L. C. Gershman. 1988. Tight binding of divalent cations to monomeric actin. *J. Biol. Chem.* 262:4952–4957.
10. Frieden, C., and K. Patane. 1987. A mechanism for nucleotide exchange in monomeric actin. *Biochemistry.* In press.
11. Harris, H. 1985. Covalent complexes formed between plasma gelsolin and actin with a zero-length cross-linking compound. *Biochemistry.* 24: 6613–6618.
12. Harris, H. E. 1985. Lack of nucleotide cleavage on the binding of G-actin-ATP to plasma gelsolin. *FEBS (Fed. Eur. Biochem. Soc.) Lett.* 190: 81–83.
13. Janmey, P. A., C. Chaponnier, S. E. Lind, K. S. Zaner, T. P. Stossel, and H. L. Yin. 1985. Interactions of gelsolin and gelsolin-actin complexes with actin. Effects of calcium on actin nucleation, filament severing, and end blocking. *Biochemistry.* 24:3714–3723.
14. Jericevic, Z., D. M. Benson, J. Bryan, and L. C. Smith. 1987. Rigorous convergence algorithm for fitting a monoexponential function with a background term using the least squares method. *Anal. Chem.* 59: 658–662.
15. Kurth, M. C., L.-L. Wang, J. Dingus, and J. Bryan. 1983. Purification and characterization of a gelsolin-actin complex from human platelets: evidence for Ca^{++} insensitive functions. *J. Biol. Chem.* 258:10895–10903.
16. Kwiatkowski, D. J., P. A. Janmey, J. E. Mole, and H. L. Yin. 1985. Isolation and properties of two actin-binding domains in gelsolin. *J. Biol. Chem.* 260:15232–15238.
17. Kwiatkowski, D. J., T. P. Stossel, S. H. Orkin, J. E. Mole, H. R. Colten, and H. L. Yin. 1986. Plasma and cytoplasmic gelsolins are encoded by a single gene and contain a duplicated actin-binding domain. *Nature (Lond.).* 323:455–458.
18. MacClean-Fletcher, S., and T. D. Pollard. 1980. Identification of a factor in conventional muscle actin preparations which inhibits actin filament self-association. *Biochem. Biophys. Res. Commun.* 96:18–27.
19. Magne, A., D. Gerard, L. Hirth, and G. Laustriat. 1977. Fluorescence study of tobacco mosaic virus protein. *Biochim. Biophys. Acta.* 495: 189–194.
20. Miki, M., H. Ohnuma, and K. Mihashi. 1974. Interactions of actin water e-ATP. *FEBS (Fed. Eur. Biochem. Soc.) Lett.* 46:17–19.
21. Mockrin, S. C., and E. D. Korn. 1980. Acanthamoeba profilin interacts

with G-actin to increase the rate of exchange of actin-bound adenosine 5′-triphosphate. *Biochemistry.* 19:5359–5362.
22. Neidl, C., and J. Engel. 1979. Exchange of ADP, ATP and 1:N^6-Ethenoadenosine 5′-triphosphate G-actin. *Eur. J. Biochem.* 101:163–169.
23. Porte, F., and M. Harricane. 1986. Interactions of plasma gelsolin with actin. Isolation and characterization of binary and ternary plasma-gelsolin-actin complexes. *Eur. J. Biochem.* 154:87–93.
24. Secrist III, J. A., J. R. Barrio, N. J. Leonard, and G. Weber. 1972. Fluorescent modification of adenosine containing coenzymes. Biological activities and spectroscopic properties. *Biochemistry.* 11:3499–3506.
25. Selve, N., and A. Wegner. 1986. Rate constants and equilibrium constants for binding of the gelsolin-actin complex to the barbed ends of actin filaments in the presence and absence of calcium. *Eur. J. Biochem.* 160: 379–387.
26. Tellam, R. L. 1986. Gelsolin inhibits nucleotide exchange from actin. *Biochemistry.* 25:5799–5804.
27. Thames, K. E., H. C. Cheung, and S. C. Harvey. 1974. Binding of 1,N^6-Ethanoadenosine triphosphate to actin. *Biochem. Biophys. Res. Commun.* 60:1252–1261.
28. Waechter, F. 1975. The influence of Ca^{2+} on the dissociation of 1,N^6-ethenoadenosine 5′-triphosphate from actin. *Hoppe-Seyler's Z. Physiol. Chem.* 356:1821–1822.
29. Waechter, F., and J. Engel. 1975. The kinetics of the exchange of G-actin-bound 1:N^6-Ethenoadenosine 5′-Triphosphate with ATP as followed by fluorescence. *Eur. J. Biochem.* 57:453–459.
30. Waechter, F., and J. Engel. 1977. Association kinetics and binding constants of nucleoside triphosphates with G-actin. *Eur. J. Biochem.* 74: 227–232.
31. Weeds, A. G., H. Harris, W. Gratzer, and J. Gooch. 1986. Interactions of pig plasma gelsolin with G-actin. *Eur. J. Biochem.* 161:77–84.
32. Yin, H. L., K. Iida, and P. A. Janmey. 1987. Identification of a polyphosphoinositide-regulated domain which mediates binding of a gelsolin to the sides of actin filaments prior to severing. *J. Cell. Biol.* 106: 805–812.
33. Zimmerle, C. T., K. Patane, and C. Frieden. 1987. Divalent cation binding to the high and low affinity sites on G-actin. *Biochemistry.* 26: 6545–6552.